JOURNAL OF Materials CHEMISTRY

Structure and magnetism in $BaLaMnO_{4+/-\delta}$ ($\delta = 0.00, 0.10$) and $Ba_xSr_{1-x}LaMnO_4$. Disappearance of magnetic order for $x > 0.30$.

Mario Bieringer*[a] and John E. Greedan[b]

[a]*Institut Laue-Langevin, 6 rue Jules Horowitz, BP 156, 38042 Grenoble Cedex 9, France. E-mail: bieringer@ill.fr*
[b]*McMaster University, Brockhouse Institute for Materials Research, 1280 Main Street West, Hamilton, Ontario, L8S 4M1, Canada*

Received 18th May 2001, Accepted 3rd December 2001
First published as an Advance Article on the web 4th January 2002

Polycrystalline samples of $BaLaMnO_4$, oxygen deficient and oxygen excess $BaLaMnO_{4\pm\delta}$ and the solid solution $Ba_xSr_{1-x}LaMnO_4$ have been prepared and investigated. Magnetic susceptibility, powder X-ray diffraction and variable temperature powder neutron diffraction data are presented for these compounds. $BaLaMnO_4$ and $BaLaMnO_{3.89}$ crystallize in space group *I*4/*mmm* with unit cell constants $a = 3.90252(6)$ Å, $c = 13.2660(3)$ Å and $a = 3.9089(1)$ Å, $c = 13.3243(5)$ Å. The unit cell constants for the tetragonal $BaLaMnO_{4.1}$ are $a = 3.9314(2)$ Å, $c = 13.051(1)$ Å. For the $\delta = 0.00$ compound a small ferromagnetic response appears in the susceptibility below 300 K and the Curie–Weiss $\theta = +5$ K but no evidence for long range magnetic order of any type is seen above 6 K in neutron diffraction data.

The ferromagnetic response is supressed in the reduced form, $BaLaMnO_{3.89}$, but is enhanced in the oxidized form, $BaLaMnO_{4.1}$, with the ferromagnetic onset moving to 350 K. The solid solution $Ba_xSr_{1-x}LaMnO_4$ ($0.00 \leqslant x \leqslant 0.34$) also crystallizes in space group *I*4/*mmm*. We find antiferromagnetic long range ordering for $SrLaMnO_4$ ($x = 0.0$), ordering vector $\mathbf{k} = [1/2\ 1/2\ 0]$, with $T_N = 128$ K and a Mn^{3+} moment of 3.3 μ_B, contrary to a previous report. The Nèel temperatures and ordered moment magnitudes decrease as the Ba concentration is increased from $x = 0.00$ to $x = 0.29$. For $x > 0.29$ all signs of antiferromagnetic long range order vanish. An explanation for the destruction of three-dimensional (3D) magnetic long range ordering is proposed based on the distance dependence of the 2D in-plane correlation length, the interplanar exchange coupling and competing interactions.

Introduction

Two potentially interesting perovskite-related manganates which have received relatively little attention during the recent rediscovery of this class of oxides are the K_2NiF_4 structure materials $SrLaMnO_4$ and $BaLaMnO_4$. Both compounds are reported[1] to crystallize in the ideal, tetragonal *I*4/*mmm* structure, Fig. 1. The K_2NiF_4 structure is an intergrowth of perovskite and rock salt layers, and the interfacial misfit between the two leads to a significant tetragonal distortion at the transition metal site. With the presence of the Jahn–Teller active Mn^{3+} ion at this site one would expect enhancement of this effect for both materials.

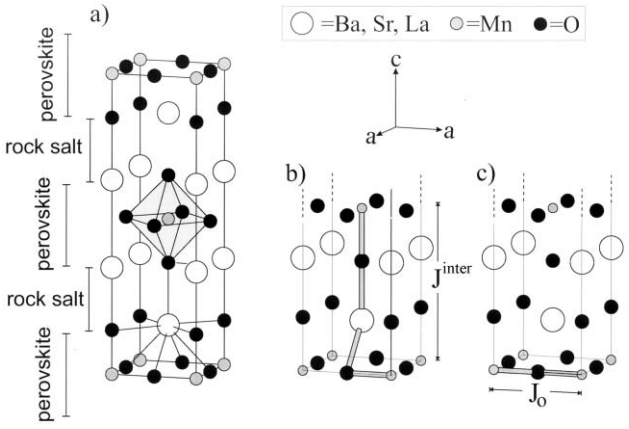

Fig. 1 a) Crystallographic structure of $BaLaMnO_4$ and $SrLaMnO_4$ – the building blocks of the layered structure are indicated on the left-hand side. Parts b) and c) show the potential interlayer and intralayer magnetic exchange paths with coupling constant J^{inter} and J_0, respectively.

The Mn^{3+} sublattice consists of square planar layers stacked in an I-centered sequence which introduces frustration into the interlayer magnetic coupling. Owing to this lattice topology, K_2NiF_4 structure compounds have long been studied as nearly canonical examples of two-dimensional antiferromagnets.[2]

Studies of the magnetic properties of $SrLaMnO_4$ and $BaLaMnO_4$ have been sparse and conflicting. In one report $SrLaMnO_4$ is claimed to develop long range antiferromagnetic order below 180 K whereas in another, T_N is placed at *ca.* 120 K.[3,4] Furthermore, the ordered magnetic moment at the Mn^{3+} site, determined from powder neutron diffraction studies, was reported as 0.80 μ_B, significantly smaller than the spin-only value of *ca.* 4.0 μ_B.[3] No magnetic properties have been published for $BaLaMnO_4$. Very recently, core-level spectroscopic studies of $SrLaMnO_4$ have been reported but these results do not aid in the resolution of the conflicts regarding the magnetism of this material.[5,6]

In this study the structure and magnetic properties of $SrLaMnO_4$ and $BaLaMnO_4$ are re-examined along with the solid solution $Ba_xSr_{1-x}LaMnO_4$. Also the oxygen excess and oxygen deficient samples of general composition $BaLaMnO_{4+\delta}$ are investigated.

Experimental

Sample preparation

Preparation of $Ba_xSr_{1-x}LaMnO_4$ ($0.00 \leqslant x \leqslant 1.00$). All samples of the series $Ba_xSr_{1-x}LaMnO_4$ were prepared from

$BaCO_3$ (99.7% Baker Chemical Co.), $SrCO_3$ (99.5% Baker Chemical Co.), La_2O_3 (99.99% Rhone-Poulenc) and Mn_2O_3 (99.9% CERAC). Residual water in $BaCO_3$ and $SrCO_3$ was determined by weight loss at 600 °C in air, the used masses being adjusted accordingly. La_2O_3 was prefired at approximately 1050 °C in air. Stoichiometric amounts of the starting materials were ground and mixed in an alumina mill with alumina grinding media in acetone. The pressed pellets were placed on Pt-foil in an Al_2O_3 boat and fired for 24 h at 1350 °C in high purity Ar. In order to assure consistent sample preparation conditions for different x-values a pellet of $BaLaMnO_4$ was simultaneously prepared as a control. Samples with $x = 0.00$, 0.06, 0.11, 0.15, 0.21, 0.23, 0.29 and 0.34 were prepared according to eqn (1). All samples had a homogeneous grey to black color and were poor electronic conductors.

$$x\ BaCO_3 + (1-x)\ SrCO_3 + {}^1/_2\ La_2O_3 + {}^1/_2\ Mn_2O_3 \rightarrow Ba_xSr_{(1-x)}LaMnO_4 + CO_2 \quad (1)$$

Preparation of $BaLaMnO_{4+\delta}$. The polycrystalline $BaLaMnO_4$ samples were pelletized, wrapped in Pt-foil and heated to 500 °C in a sealed glass tube in the presence of a stoichiometric amount of CrO_3. According to eqn (2) the chromium trioxide decomposes and the released oxygen can react with $BaLaMnO_4$ according to reaction (3).

$$2CrO_3 \xrightarrow{500^\circ C} Cr_2O_3 + 3/2O_2 \quad (2)$$

$$BaLaMnO_4 + \frac{\delta}{2}\ O_2 \xrightarrow{500^\circ C} BaLaMnO_{4+\delta} \quad (3)$$

One sample was also prepared at 500 °C in oxygen flow for 12 h, reaction (3).

Preparation of $BaLaMnO_{4-\delta}$. $BaLaMnO_4$ samples were reduced using H_2 gas at various partial pressures and temperatures. The unit cell constants of the resulting products were monitored and correlated with the reaction conditions but the absolute degree of reduction could not be obtained directly. Reaction (4) summarizes the overall reaction.

$$BaLaMnO_4 + \delta\ H_2 \xrightarrow{T,p} BaLaMnO_{4-\delta} + \delta\ H_2O \quad (4)$$

Elemental analysis

Samples of approximately 150 mg were dissolved in 1–2 ml freshly prepared hot *aqua regia* and the concentrated solutions were diluted to appropriate concentrations with distilled water. The elemental analysis was carried out using an atomic emission spectrometer with inductively coupled plasma, ICAP–9000 Fisher Scientific Instruments.

Magnetic measurements

Bulk magnetic susceptibility measurements were performed using a Quantum Design MPMS SQUID magnetometer in the temperature range from 5 to 350 K and an applied magnetic field of 0.01 T. The samples were contained in gelatine capsules held in plastic straws. High-temperature measurements were carried out in quartz tubes between 300 and 600 K using a furnace insert.

X-Ray powder diffraction

Room temperature powder X-ray diffraction patterns were obtained using a Guinier-Hägg camera having $CuK\alpha_1$ radiation ($\lambda = 1.54056$ Å) and using silicon as an internal standard.

Powder neutron diffraction

Low resolution neutron powder diffraction experiments were carried out in the temperature range $T = 10$–150 K on the powder diffractometer at the McMaster Nuclear Reactor using a neutron wavelength $\lambda = 1.392$ Å. The sample was measured in a He-filled aluminium sample can sealed with an indium gasket.

High resolution low temperature powder neutron diffraction experiments were performed on the C2 diffractometer (800 wire position sensitive detector) operated by the Neutron Program for Materials Research of the National Research Council of Canada at the Chalk River Nuclear Laboratory. The powder patterns were taken in a vanadium sample can using neutron wavelengths $\lambda = 1.3263$ and 2.3692 Å over the 2θ range 5–85°.

Room temperature time of flight (TOF) neutron powder diffraction data were collected at IPNS at the Argonne National Laboratory on instrument SEPD using a vanadium sample can over the d-spacing range 0.4–4.0 Å. All powder diffraction data were analyzed using the Rietveld refinement program GSAS.[7] Bond valence calculations were carried out according to Brown and Altermatt[8] using eqns. (5) and (6).

$$S_i = \exp((R_i - R_0)/b) \quad (5)$$

$$V = \sum_i S_i \quad (6)$$

The bond valence S_i for bond i is determined from the bond distance R_i and tabulated R_0 values and with parameter $b = 0.37$. The bond valence sum V is the sum of all i bond valences S_i of the coordination sphere.

Results and discussion

$SrLaMnO_4$

The unit cell constants of the sample prepared here, $a = 3.7979(3)$ Å and $c = 13.102(1)$ Å, compare well with values from the literature for stoichiometric $SrLaMnO_{4+\delta}$, where $\delta \approx 0.0$.[1,4] Neutron diffraction data taken on a powder sample at 10 K are shown in Fig. 2 along with simulated powder patterns for Mn^{3+} moments of 0.80 μ_B, as claimed in ref. 3 and for 3.3 μ_B, assuming in both cases the $\mathbf{k} = [1/2\ 1/2\ 0]$ magnetic structure found commonly for K_2NiF_4 structure materials. The data, which are essentially indistinguishable from those of ref. 3, are consistent with the larger moment rather than the smaller. This value is also much closer to the spin-only moment of 4.0 μ_B and is a more reasonable result. Also, on the right-hand side in Fig. 2 the temperature dependence of the Mn^{3+} moment, derived from neutron diffraction data, is plotted and is consistent with $T_N = 128(2)$ K, much closer to the 120 K value of ref. 4 than the 180 K value of ref. 3

$BaLaMnO_{4+/-\delta}$

This material was first reported in 1977 to crystallize in the K_2NiF_4 structure with unit cell constants $a = 3.902(5)$ Å and $c = 13.27(1)$ Å, but a detailed structure was not refined nor were any properties described.[1] An effort was made to explore the range of oxygen non-stoichiometry in this compound. A sample prepared under conditions neutral to oxidation or to reduction was found to have unit cell constants very near to the reported values, $a = 3.90252(6)$ Å and $c = 13.2660(3)$ Å for which a nominal value of $\delta = 0.00$ can be assigned. According to eqns. (2) and (3) this sample was oxidized at 500 °C using accurate amounts of CrO_3 as an oxygen source. The results are shown in Fig. 3 where it is seen that the a-axis increases with oxidation while the c-axis decreases. The relative independence of the tetragonal cell constants $a = 3.9314(2)$ Å and $c = 13.051(1)$ Å beyond an addition of $\delta = +0.10$ oxygen according to eqn. (3) suggests that this value is close to the

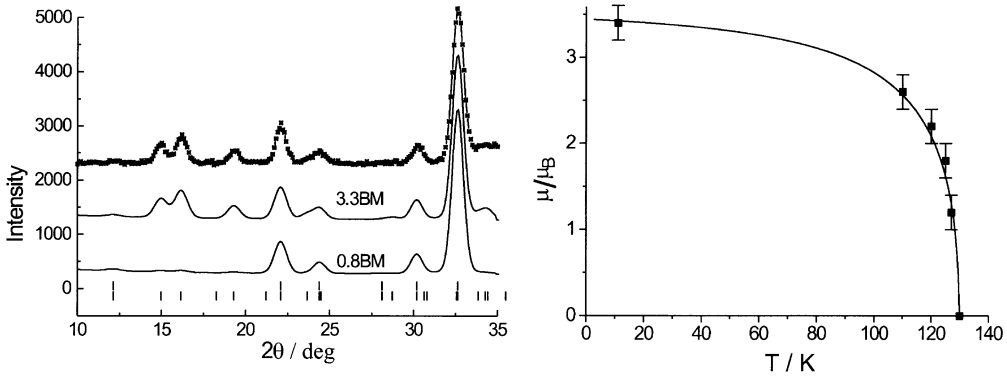

Fig. 2 Left: experimental (uppermost pattern) neutron powder diffraction pattern ($\lambda = 1.392$ Å) for $SrLaMnO_4$ ($T = 10$ K) and simulated patterns for a magnetic moment of 3.3BM and 0.8BM. The upper and lower sets of tick marks refer to the nuclear and magnetic Bragg peak positions, respectively. Right: evolution of the refined magnetic moment magnitude for $SrLaMnO_4$.

upper limit. It is assumed that a quantitative reaction between $BaLaMnO_4$ and supplied oxygen takes place for δ values $\leqslant 0.1$. If oxygen is supplied in excess of $\delta = 0.1$ then the additional oxygen is not incorporated into the $BaLaMnO_4$ structure. However, the quantity δ must be understood as a nominal value because our analysis does not permit an absolute quantification of excess oxygen in $BaLaMnO_{4\ +/-\ \delta}$. Thermal gravimetric analysis (TGA) did not allow the determination of oxygen in the samples because it was not possible to oxidize or reduce the samples in a controlled fashion, due perhaps to the formation of stable, undefined intermediate products. The samples are only soluble in hot *aqua regia*, which prevents the determination of the oxygen content by titration. We would like to point out that limiting levels of oxygen excess, close to our estimated values for $BaLaMnO_{4\ +/-\ \delta}$, have been observed in related K_2NiF_4 structure oxides such as $La_2CuO_{4\ +\ \delta}$ ($\delta = +0.13$) and $La_2NiO_{4\ +\ \delta}$ ($\delta = +0.17$).[9,10] In these materials the excess oxide ion is found to reside in the rock salt layer. The observed increase in cell volume $V = 203.74(2)$ Å^3 for the nominal $\delta = 0.10$ material compared with 202.036(6) Å^3 for the $\delta = 0.00$ sample, is consistent with an oxide interstitial in $BaLaMnO_{4.1}$.

However, a sample heated in pure oxygen at 500 °C for 12 h was found to be tetragonal with unit cell parameters $a = 3.9553(1)$ Å and $c = 13.0230(5)$ Å based on Guinier X-ray diffraction data. The further increase of the a-axis and the decrease of the c-axis parameters suggest an oxidation beyond $\delta = 0.1$, and the total mass gain during oxidation suggests an overall composition of $BaLaMnO_{4.3}$. It appears that a large excess of oxygen gas is required in order to allow additional oxygen uptake by the sample, whereas two-fold excess is not sufficient to oxidize beyond $BaLaMnO_{4.1}$. However, time of flight powder neutron diffraction data show that the space group symmetry is lower than *I*4/*mmm*, that phase segregation has occured, and that an unidentified impurity phase is present.

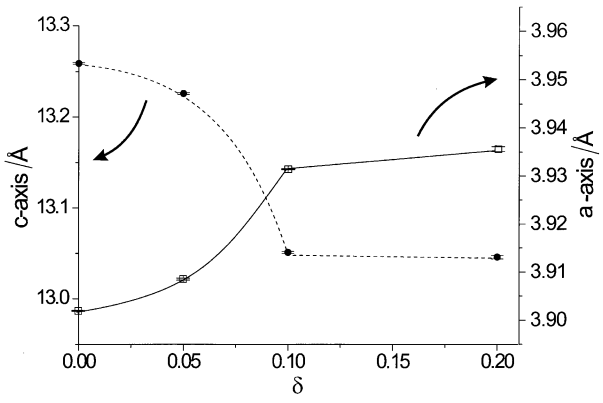

Fig. 3 Unit cell constants a (□) and c (●) for $BaLaMnO_{4\ +\ \delta}$, where δ is the nominal oxygen content.

In addition to the oxidized phases, a reduced sample was prepared by heating the $\delta = 0.00$ sample under H_2 for 12 h at 500 °C. The resulting cell constants are $a = 3.9089(1)$ Å and $c = 13.3243(5)$ Å, giving also a slightly larger cell volume, 203.59(2) Å^3, than the stoichiometric phase. As will be shown later, for this sample $\delta = -0.11(2)$. The increased cell volume here is also reasonable due to the greater radius of Mn^{2+} which is introduced due to the oxygen deficiency.

Room temperature neutron diffraction data were collected and refined for the stoichiometric and oxygen deficient samples (Fig. 4). The results for both materials, including derived interatomic distances, are listed in Table 1. In the case of the nominally stoichiometric compound, there is some evidence for a very slight vacancy concentration on the Ba,La site but at a level just barely above the statistical error. To within error, the Mn site appears to be fully occupied. The refined composition is, therefore, $(BaLa)_{1.98(1)}MnO_4$. For the reduced phase, the expected increase in average Mn–O distance and the corresponding decrease in the bond valence at the Mn site with respect to the $\delta = 0.00$ sample are observed. There is also some evidence that the oxygen deficiency is localized at the O(2) site at 1/2, 0, 0. The refined composition is, then, $BaLaMnO_{3.89(2)}$.

Attempts to refine the time of flight powder neutron diffraction data for the oxidized sample, prepared in oxygen flow at 500 °C, were less successful due to the presence of broad, diffuse features associated with the strong reflections, which prevented a meaningful refinement. This suggests a greater level of disorder or diminished crystallinity for this sample. It is possible to index most peaks using two phases (space groups *I*4/*mmm* and *Bmab*); however, the sample cannot be considered pure which is in agreement with the fact that the oxygen uptake is far above the upper limit of $\delta = +0.1$.

The phase purity of the $BaLaMnO_{4\ +/-\ \delta}$ samples was assessed by Guinier X-ray diffraction. The nominally $\delta = 0.00$ material appeared to contain a small amount of the oxidized form, and an upper limit of 2% is estimated.

The bulk magnetic properties of the three $BaLaMnO_{4\ +/-\ \delta}$, just described, are shown in Fig. 5. for the range *ca.* 2–350 K. To our knowledge, such data have not been reported before for any form of $BaLaMnO_4$. Beginning with the $\delta = 0.00$ material, a weakly ferromagnetic response is seen to develop below about 300 K and at low temperatures a weak maximum below 25 K. The ferromagnetic signal is clearly enhanced in the oxidized form and much diminished in the reduced form. In all three cases, the low temperature maximum persists. Fig. 5 shows only the zero-field cooled (ZFC) data for clarity. In the field-cooled (FC) data, FC–ZFC divergences occur at about 290 K for $\delta = 0.00$, at 350 K for $\delta = +0.10$ and 265 K for

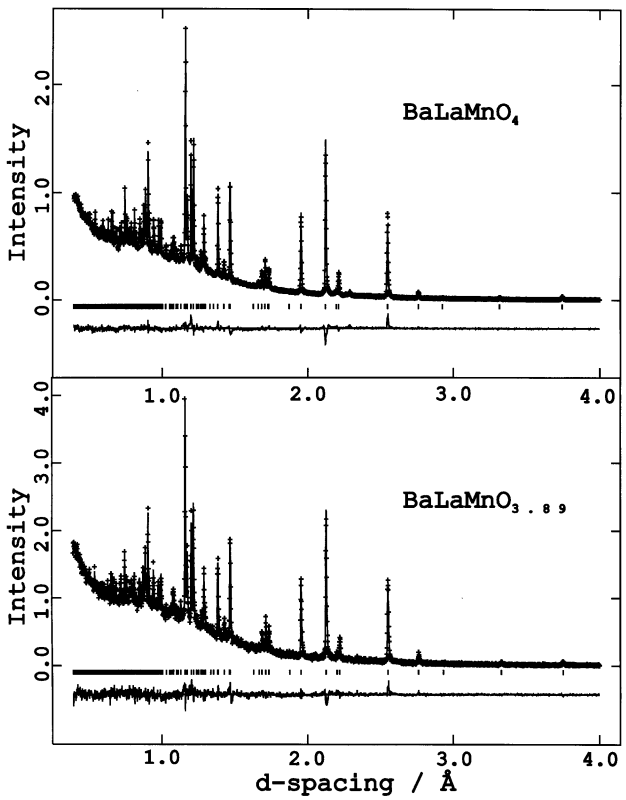

Fig. 4 Rietveld refinements for $BaLaMnO_4$ (upper frame) and $BaLaMnO_{3.89}$ (lower frame) using time of flight (TOF) powder neutron diffraction data. The crosses are the experimental data, the solid lines through the data points are the best fits, the tick marks indicate nuclear Bragg peaks and the lower solid line represents the difference between experimental data and the fitted model.

Table 1 Rietveld refinement results for $BaLaMnO_4$ and $BaLaMnO_{4-\delta}$ (with $\delta \approx 0.1$) using room temperature time of flight neutron data. The space group is *I*4/*mmm*. The bond valence sums were calculated according to eqns. (5) and (6)

	$BaLaMnO_4$	$BaLaMnO_{4-\delta}$
No. of profile points	5402	5499
No. of parameters	25	30
a/Å	3.90252(6)	3.9089(1)
c/Å	13.2660(3)	13.3243(5)
V/Å^3	202.036(6)	203.59(2)
R_{wp} (%)	6.83	8.95
R_p (%)	3.88	5.41
Reduced χ^2	3.73	1.377
Atomic positions		
	$BaLaMnO_4$	**$BaLaMnO_{4-\delta}$**
Ba,La (0 0 *z*)	$z = 0.35735(10)$	$z = 0.35648(16)$
$U_{iso}/U_e \times 100$	0.80(7)	1.03(8)
Occupation	0.990(3)	1.0
Mn (0 0 0)		
$U_{iso}/U_e \times 100$	0.72(7)	1.17(12)
Occupation	0.990(7)	1.0
O(1) (0 0 *z*)	$z = 0.16841(14)$	$z = 0.16968(21)$
$U_{iso}/U_e \times 100$	3.829(11)	3.88(12)
Occupation	1.0	1.0
O(2) (1/2 0 0)		
U_{iso}/U_e	1.87(11)	2.38(12)
Occupation	1.0	0.944(13)
Selected interatomic distances/Å		
Mn–O(1) × 2	2.2341(19)	2.2608(28)
Mn–O(2) × 4	1.95126(3)	1.9544(1)
$<$Mn–O$>_{(ave.)}$	2.05	2.06
Ba–O(1) × 1	2.5065(21)	2.4891(32)
Ba–O(1) × 4	2.78057(31)	2.7859(5)
Ba–O(2) × 4	2.7182(9)	2.7343(15)
Bond valence sums		
Ba : La	2.47	2.43
Mn	2.94	2.88

$\delta = -0.11$, where the reduced phase, and the low temperature maxima are surpressed. These FC–ZFC divergences at low temperature may signal the formation of a spin glass like magnetic phase but more work is needed to establish this.

These results are at least qualitatively consistent with expectations, as the oxidized form, nominally $BaLaMnO_{4.1}$, will contain *ca.* 20% Mn^{4+} and domains in which ferromagnetic Mn^{3+}–Mn^{4+} (d^4–d^3) double exchange can operate will exist. As noted, the nominally $\delta = 0.00$ phase may contain a small amount of the oxidized phase as an impurity and this could account in part for the weak ferromagnetic response. The reduced sample will contain only Mn^{2+} and Mn^{3+} and ferromagnetic exchange will be weaker, and if present at all will be due to (d^5–d^4) superexchange which can be weakly ferromagnetic.[11]

Data for the $\delta = 0.00$ sample were collected at higher temperatures, 300–600 K, and an apparent Curie–Weiss regime was found, inset Fig. 5, yielding fitting constants $\mu_{eff} = 5.18(3)$ μ_B and $\theta_c = +5(2)$ K. The μ_{eff} value is slightly greater than the spin-only value of 4.90 μ_B and the slightly positive θ_c value is not inconsistent with the observed weak ferromagnetic behavior.

Evidence for either long range or short range magnetic order can be obtained, in principle, from neutron diffraction experiments. For the $\delta = 0.00$ sample, data were collected both at low temperature, 6 K, and at room temperature, 294 K, with $\lambda = 2.3962$ Å neutrons over a 2θ interval from 5 to 85°. This covers a range of observable *d*-spacings out to 27.5 Å. Fig. 6 shows results at both temperatures along with a difference plot, 6–294 K. As is clear, there are no new features in the 6 K dataset which would signal long range (resolution limited Bragg peaks) or even short range (broad peaks) magnetic order. The contrast with the corresponding data for $SrLaMnO_4$, Fig. 2, is striking, given the identical crystal structures, similar chemistry and unit cell dimensions. The remarkable conclusion is, then, that $BaLaMnO_4$ shows no obvious sign of magnetic order of any kind over the *d*-spacing and temperature range explored here.

$Ba_xSr_{1-x}LaMnO_4$

The striking contrast between the magnetic properties of $SrLaMnO_4$ and $BaLaMnO_4$ prompted an investigation of the solid solution $Ba_xSr_{1-x}LaMnO_4$. Samples covering the compositional range $x = 0.06$–0.34 were prepared and characterized by X-ray and neutron powder diffraction and bulk susceptibility measurements. The cation content in the

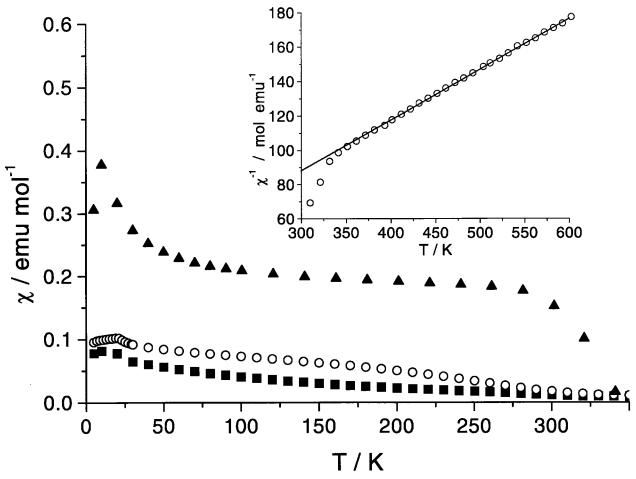

Fig. 5 Zero-field cooled magnetic susceptibility data for $BaLaMnO_{4+\delta}$ [$\delta = -0.11$(■), 0.00 (○) and +0.10 (▲)], using a magnetic field $H = 0.01$ T. The inset shows the inverse d.c. magnetic susceptibility data points for $BaLaMnO_4$ collected at high temperatures, where the solid line represents the best fit to the Curie–Weiss law.

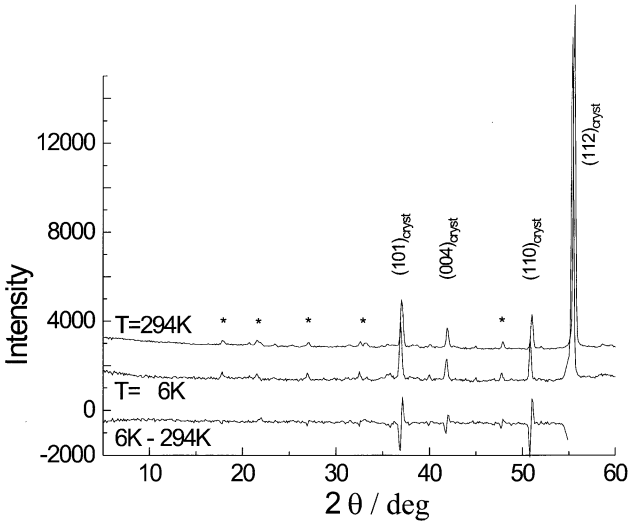

Fig. 6 Continuous wave powder neutron diffraction data for $BaLaMnO_4$ ($\lambda = 2.3692$ Å). The stars show crystallographic reflections caused by a minor impurity which has not been identified.

products was also determined by atomic emission spectroscopy (AES).

The unit cell constants derived from Guinier X-ray data are summarized in Table 2. For all compositions the ideal *I*4/*mmm* structure is retained as expected. The unit cell volume increases linearly with the composition x (Fig. 7). Bulk susceptibility data for the low temperature regime, 5–300 K, are shown in Fig. 8. In all cases the molar susceptibilities are lower than for any of the $BaLaMnO_4$ samples studied, there is no evidence for a ferromagnetic response, and a distinct χ_{max} is evident at relatively high temperatures followed by a Curie-like tail at the lowest temperatures. Also, not shown are data taken over the range 300–600 K on the same samples. In this regime a Curie–Weiss behavior was found in all cases. The data from both thermal regimes are collected in Table 3. For all x, the μ_{eff} values are near the spin-only value of 4.90 μ_B for Mn^{3+}, the θ_c values are all negative in contrast to $BaLaMnO_4$ but show no clear trend while the $T(\chi_{max})$ do decrease systematically with increasing x. It is likely that the maxima can be associated with T_c or T_N, *i.e.* a transition to an AF ground state, but this must be verified by neutron diffraction. The fact that θ_c is systematically smaller than the $T(\chi_{max})$ for all series members indicates the presence of competing AF and F exchange constraints. It also appears that the susceptibilities at the lowest temperatures increase with increasing x, and that this is accompanied by an increase in the divergence between the FC and ZFC data. Note the absence of a broad maximum which might be expected for short range 2D correlated AF spins.

Neutron diffraction data for the $Ba_xSr_{1-x}LaMnO_4$ series were collected on the C2 diffractometer for compositions $x =$ 0.06, 0.11, 0.15, 0.21, 0.23, 0.29 and 0.34 at several temperatures. The results for $x = 0.06$ are typical for the series up to $x = 0.29$ and are shown in Figs. 9 and 10. Examination of the low angle data, Fig. 9, discloses evidence for long range order

Table 2 Unit cell constants and cell volumes for $Ba_xSr_{1-x}LaMnO_4$ [Ba content (x) determined by atomic emission spectroscopy (AES)]

Ba (x) from AES	a/Å	c/Å	V/Å^3
0.00	3.804(5)	13.10(1)	189.6(6)
0.06(2)	3.7982(2)	13.136(1)	189.50(3)
0.11(2)	3.8033(2)	13.133(1)	189.97(3)
0.15(2)	3.8095(2)	13.136(1)	190.63(3)
0.21(2)	3.8190(2)	13.134(1)	191.56(3)
0.23(2)	3.8169(2)	13.1387(8)	191.41(3)
0.29(2)	3.8229(2)	13.143(1)	192.07(4)
0.34(2)	3.8337(4)	13.144(2)	193.18(7)

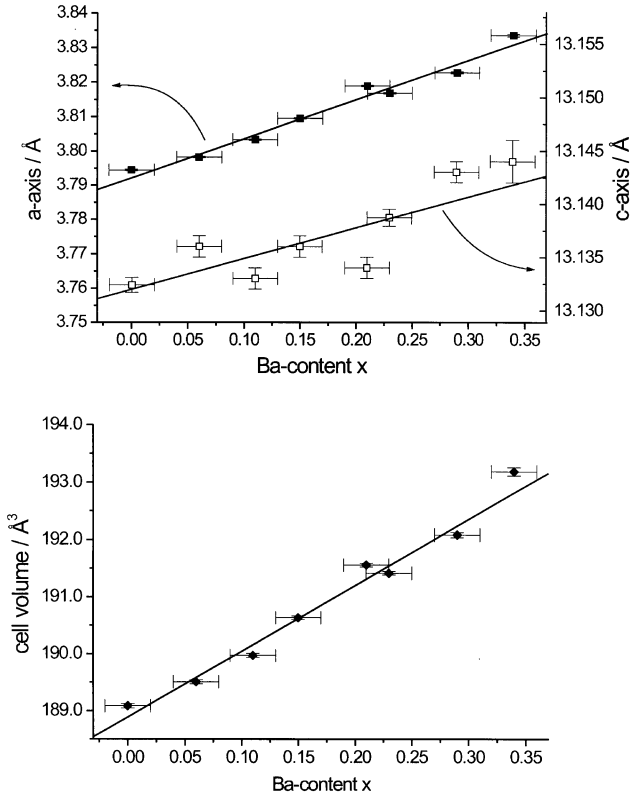

Fig. 7 Top: tetragonal unit cell constants for $Ba_xSr_{1-x}LaMnO_4$ as a function of x. Bottom: unit cell volume *versus* x (x values determined from atomic emission spectroscopy, a and c axes determined from Guiner X-ray patterns).

at low temperatures in the appearance of reflections of the type (1 0 l), where $l = 0,1,2,3,\cdots$, indexed on a tetragonal magnetic supercell, $\mathbf{a}_{mag} = \sqrt{2}\mathbf{a}_{nucl}$. This is the $\mathbf{k} = (1/2\ 1/2\ 0)$ magnetic structure often found for K_2NiF_4-type materials. In Fig. 10 a combined nuclear–magnetic structure refinement is shown for the $x = 0.06$ phase, indicating an excellent fit to the proposed model which is shown on the right-hand side of the figure. Fits of similar quality are obtained for all compositions with $x < 0.34$, confirming the same model for the magnetic structure for all x. The refined Mn^{3+} magnetic moments at the lowest temperature studied for each x are collected in Table 4 along with the agreement indices. More complete results appear in Fig. 11, where the thermal evolution of the refined Mn moment is shown for $x = 0.06$ to 0.29 on the left-hand side of the figure. Note the remarkable reduction in the ordered moment and T_c as x increases to 0.29. It is important to recall that the nominal Mn oxidation state remains constant throughout at +3, $S = 2$ and $\mu_{ord} = 4.0\ \mu_B$, so the ordered moment at $x = 0.29$ is only half the expected value for $S = 2$.

For $x = 0.34$ no magnetic Bragg peaks are observed down to 2 K. The lower part of Fig. 11 compares the powder neutron diffraction data for all compositions at low temperatures, indicating the absence of long range order for $x \geqslant 0.29$. Note that the refined moment and apparent T_c for $x = 0.21$–0.29 are very similar. It is not clear at present whether this is the true behavior of this series or if some type of phase separation occurs just above $x = 0.21$. While no such effect is observable even in the relatively high resolution Guinier X-ray data, synchrotron source data would be necessary to resolve this issue. Nonetheless, the reduction in the ordered Mn^{3+} moment and the disappearance of long range magnetic order in this series can only be described as precipitous.

Further information concerning the nature of the magnetic phase transition can be obtained by analysis of the temperature dependence of the ordered moment as T_c is approached from lower temperatures. This involves fitting to a power law of the

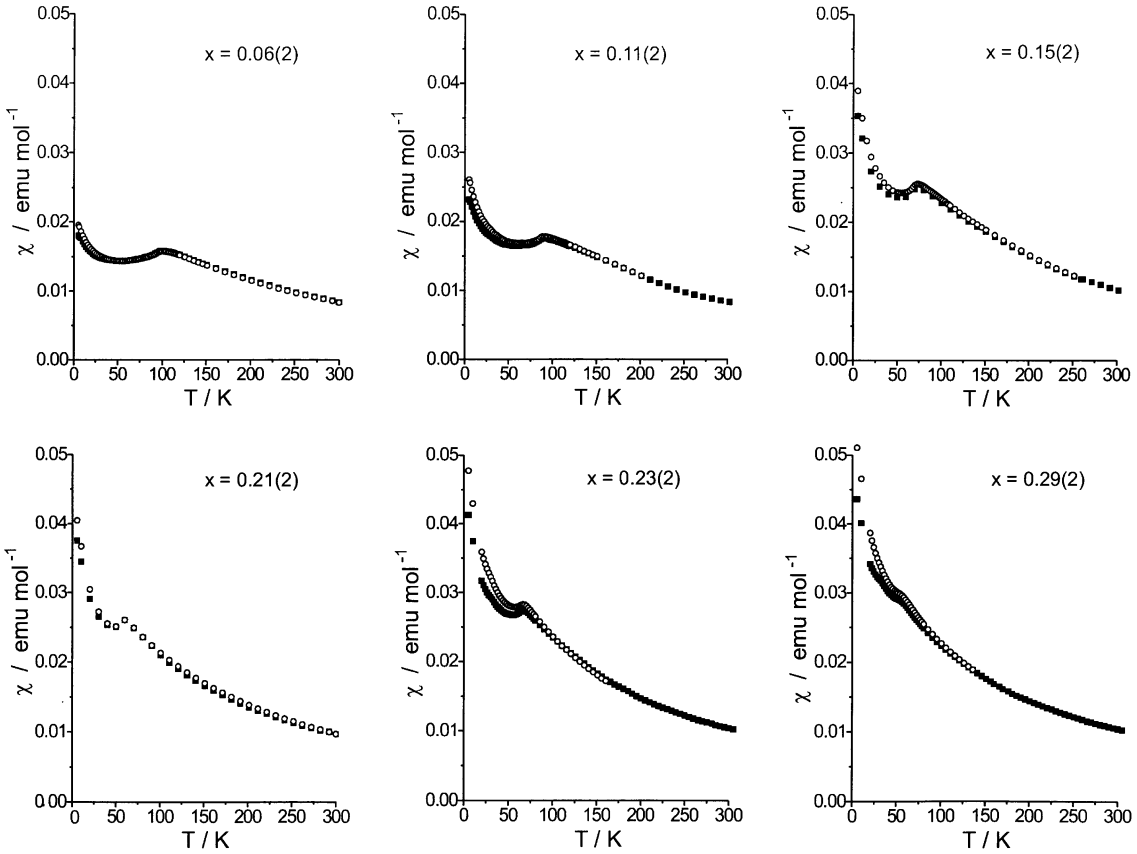

Fig. 8 Low temperature d.c. magnetic susceptibility data for $Ba_xSr_{1-x}LaMnO_4$ measured in a magnetic field $H = 0.01$ T. Solid and open symbols are ZFC and FC data sets, respectively.

Table 3 Effective magnetic moments (μ_{eff}) and Weiss temperatures (θ_c) from Curie–Weiss fits (350–600K) and $T(\chi_{max})$ for $Ba_xSr_{1-x}LaMnO_4$

x	$\mu_{eff}(\mu_B)$	θ_c/K	$T(\chi_{max})$/K
0.06(2)	5.06(2)	−89(6)	100(5)
0.11(2)	4.53(3)	−40(7)	92(2)
0.15(2)	4.61(3)	−10(1)	74(2)
0.21(2)	4.85(2)	−8(4)	65(5)
0.23(2)	5.22(10)	−39(4)	66(2)
0.29(2)	5.38(3)	−48(1)	58(2)
1.00	5.18(3)	+5(2)	—

form

$$\mu = A[(T - T_c)/T_c]^{\beta} \quad (7)$$

where β is a so-called critical exponent,[12] and μ is the magnetic moment as refined from the powder neutron diffraction data. Assuming T_c values from the susceptibility data, β values were derived from plots such as Fig. 12 and the results are collected in Table 5. Note that all values, with the exception of $x = 0.29$, lie near the range for the 2D Ising model $\beta = 0.125$. An alternative would be the 3D Ising model with a predicted $\beta = 0.326$. With our experimentally determined β values being

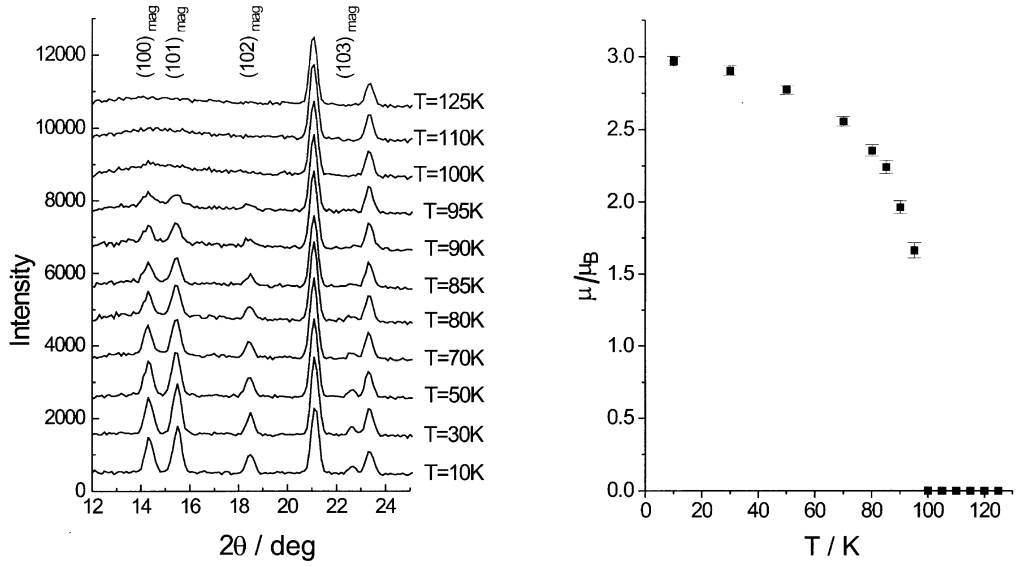

Fig. 9 Left: variable temperature powder neutron diffraction data for $Ba_{0.06}Sr_{0.94}LaMnO_4$ ($\lambda = 1.3263$ Å); the data sets are normalized. Right: temperature evolution of the magnetic moment magnitude on Mn^{3+}.

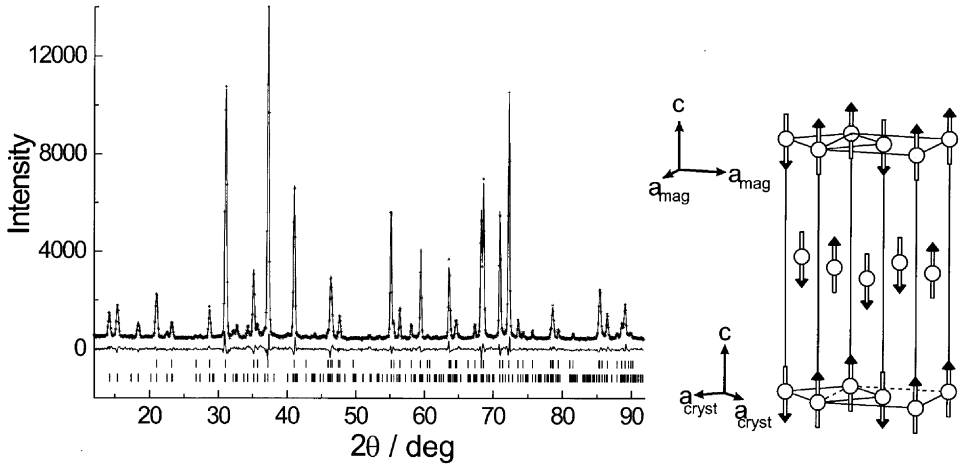

Fig. 10 Rietveld profile fit for powder neutron diffraction data for $Ba_{0.06}Sr_{0.94}LaMnO_4$ collected at $T = 10$ K ($\lambda = 1.3263$ Å). The crosses are experimental data points, the solid line through the data points is the best fit, the solid line underneath the data points is the difference curve. The upper and lower tick marks indicate nuclear and magnetic Bragg peaks, respectively. The magnetic structure model is illustrated on the right.

significantly closer to 0.125 we conclude that this system is best described as a 2D Ising magnet. Note also that the power law dependence holds for temperatures well below T_c. Data are not available quite close to T_c so the issue of cross-over effects to other exponents cannot be addressed here. It should be noted that similar behavior, *i.e.* adherence to the 2D Ising power law for a wide temperature range, is not uncommon for magnetic materials of this structure type and is indeed observed for K_2NiF_4 itself.[13]

The two-dimensionality of the magnetic correlations in these materials is also manifest in the temperature range above T_c. This is clear from Fig. 13 where low angle data are shown for several temperatures just above T_c for $Ba_{0.06}Sr_{0.94}LaMnO_4$. Magnetic diffuse scattering in the form of an asymmetric Warren line shape near the (10) position [2θ (10) = 14.5°] is evident. A fit of the Warren function[14,15] to the data at 100 K gives a 2D correlation length of 21(3) Å which varies very little with increasing temperature up to 125 K. Hints of similar behavior for other compositions in the series are present but the available data are of insufficient quality to permit a detailed analysis. Thus, the solid solutions $Ba_xSr_{1-x}LaMnO_4$ do show the expected 2D short range correlations in the neutron scattering but with a surprisingly short correlation length of order no more than *ca.* 20 Å. Recall that there was no signature of 2D short range correlations in the bulk susceptibility data above T_c.

As already remarked, the precipitous disappearance of long range order for $x > 0.29$ is difficult to understand. One might begin by recognizing the quasi-2D nature of the magnetic correlations in these materials. For such a circumstance the critical temperature for 3D ordering depends in fact on the 2D correlation length, ξ_{2D}, and the interplanar exchange coupling constant, J^{inter}, as in eqn. (8) (where k is the Boltzmann constant).[16]

$$T_c = \xi_{2D}{}^2 J^{inter} S^2/k \quad (8)$$

Table 4 Refined magnetic moments for Mn^{3+} at 10 K, extrapolated T_c values and agreement indices for $Ba_xSr_{1-x}LaMnO_4$ ($x = 0.00$ to 0.29)

x	μ_{ord}/μ_B	T_c/K	R_{wp} (%)	R_{mag} (%)
0.00	3.30	128(5)	—	—
0.06(2)	3.02(6)	100	5.99	16.5
0.11(2)	2.79(5)	92	5.58	16.4
0.15(2)	2.48(5)	74	4.77	22.2
0.21(2)	2.07(5)	65	6.47	26.8
0.23(2)	2.20(5)	70	6.02	22.6
0.29(2)	1.95(5)	62	5.17	27.0
0.34(2)	0.0	0	5.93	—

It is reasonable to assume that ξ_{2D} will depend on the intraplanar distances and J^{inter} on the interplanar distances, respectively. Of course, as the x increases in $Ba_xSr_{1-x}LaMnO_4$, both distances will increase and correspondingly, ξ_{2D}, J^{inter} and T_c will decrease. The interplanar exchange pathway involves a Mn–O–(Ba/Sr/La)–O–Mn link while the nearest neighbor (nn) intraplanar pathway is of course just the

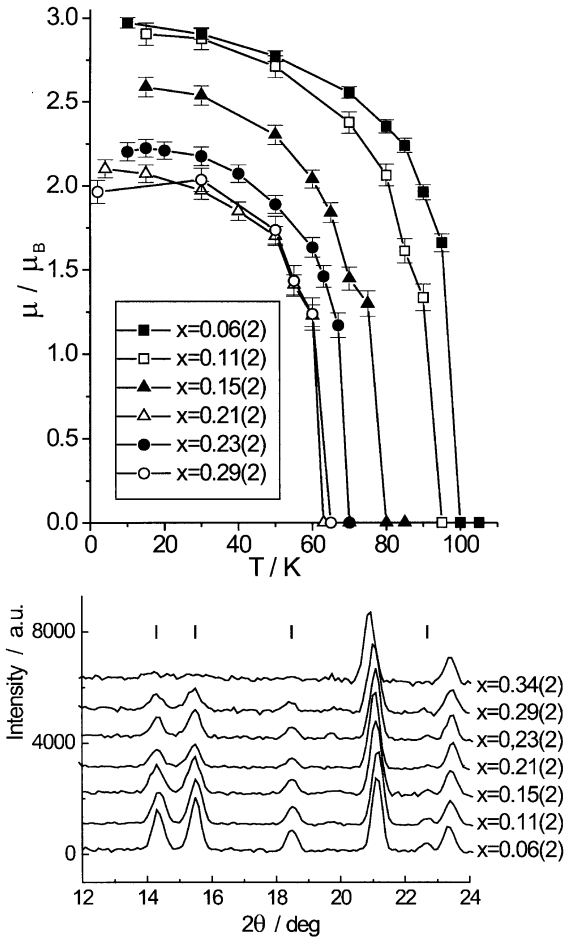

Fig. 11 Top: magnetic moment evolution for $Ba_xSr_{1-x}LaMnO_4$ for six compositions as determined using the Rietveld refinement method for neutron powder diffraction data sets. Bottom: comparison of neutron powder diffraction patterns ($\lambda = 1.33$ Å) for seven compositions for the lowest measured temperatures (2–15 K); the tick marks show the approximate positions for expected magnetic Bragg peaks.

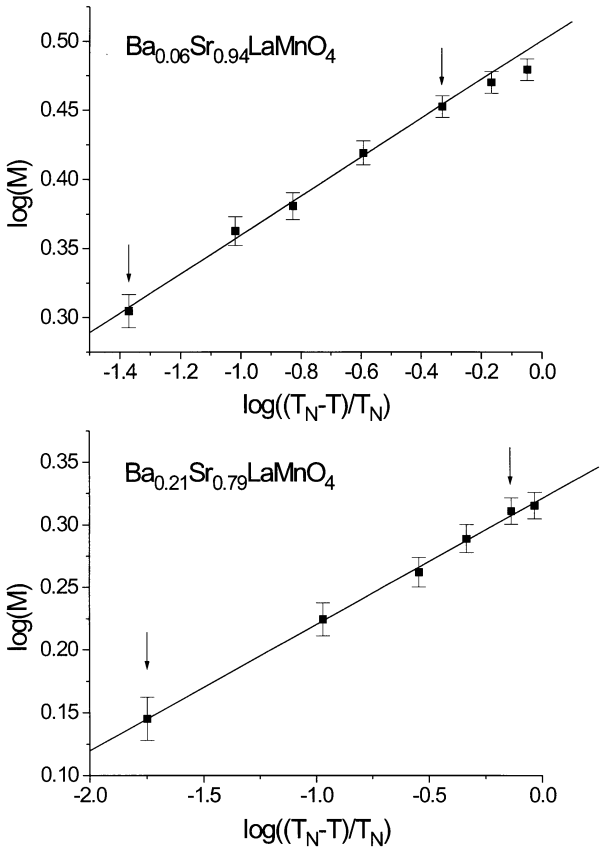

Fig. 12 Determination of critical exponents, β, from neutron diffraction experiments using log–log plots of the magnetic moment and the reduced temperature. The solid lines are the best fits according to eqn. (7); the fitting ranges are indicated with the arrows.

Mn–O–Mn link along the unit cell axis, *a*. Both pathways are shown in Fig. 1. The variation of both distances with increasing *x* is compared in Table 6. The percentage increase in the nn distance is about twice that for the interplanar distance, 0.9% for the former *versus* 0.5% for the latter as *x* increases from 0.06 to 0.34, although the absolute increases are comparable, *ca.* 0.04 Å for each. In the absence of a detailed understanding of the distance dependence of either ξ_{2D} or J^{inter} it is difficult to know which plays a greater role in the destruction of antiferromagnetic long range order (AFLRO) for $x > 0.29$. It is possible to measure ξ_{2D} by neutron scattering and such measurements should be undertaken.

Nonetheless, these structural arguments aside, electronic structure must play a fundamental role in the extreme sensitivity of this system to the demise of long range AF order. One can compare the isostructural and electronically very similar series, $MLaFeO_4$ where M = Ca, Sr and Ba. Here Fe^{3+} is in the high spin state, $t_{2g}^3e_g^2$, compared with $t_{2g}^3e_g^1$ for Mn^{3+}, and significant changes in inter- and intra-atomic Fe–Fe distances occur upon substituting the larger Ba^{2+} for the smaller Ca^{2+} and Sr^{2+} ions.[17,18] In spite of this, the magnetic properties in the Fe series change very little, T_c decreases from 383 K for Ca to 341 K for Ba, and there is no catastrophic

Table 5 Derived critical exponents β for $Ba_xSr_{1-x}LaMnO_4$

x	β	T_c/K
0.06(2)	0.141(5)	100
0.11(2)	0.142(6)	92
0.15(2)	0.113(6)	74
0.21(2)	0.101(2)	65
0.23(2)	0.176(6)	68
0.34(2)	0.221(5)	63

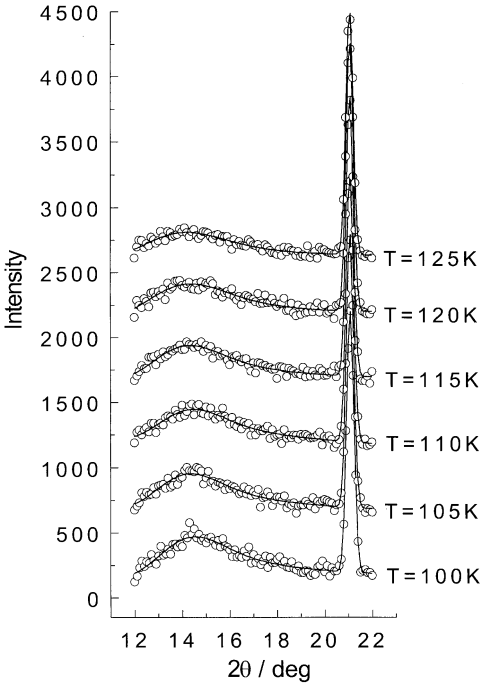

Fig. 13 Powder neutron diffraction patterns for $Ba_{0.05}Sr_{0.95}LaMnO_4$ for temperatures close to the onset of magnetic long range ordering. The broad asymmetric features indicate two-dimensional magnetic short range order; the two-dimensional magnetic correlation lengths are determined using the Warren function (solid lines).

disappearance of LRO. Another comparison may be useful. Consider the isostructural series, $SrLaMO_4$ where M = Cr, Mn and Fe. Reported T_c values for these materials are 240, 128 and 351 K, respectively.[17,18] This sequence indicates that AF interactions are significantly weaker in the Mn compound than in the adjacent Cr and Fe counterparts. Consistent with these observations, the Goodenough–Kanamori rules for 180° Mn^{3+}–Mn^{3+} superexchange predict competing AF and F interactions.[11] It is, thus, not impossible that apparently small changes in bond lengths could shift this fairly delicate balance to destabilize the AF ground state.

Summary

A study of the relatively uninvestigated K_2NiF_4 manganates, $SrLaMnO_4$ and $BaLaMnO_4$ and the solid solution $Ba_xSr_{1-x}LaMnO_4$ has revealed some remarkable magnetic behavior. Long range AF order is confirmed in $SrLaMnO_4$ but with an ordered moment of 3.3 μ_B and T_c = 128 K, in contrast to an earlier report of a much smaller moment (0.8 μ_B) and a much higher T_c (180 K). The range of oxygen non-stoichiometry in $BaLaMnO_{4+/-\delta}$ has been investigated for the first time and it is found that $\delta \approx 0.10$. Oxidizing $BaLaMnO_4$ beyond $BaLaMnO_{4.1}$ results in phase segregation and impurity formation. Stoichiometric $BaLaMnO_4$, in contrast to isostructural

Table 6 Mn–Mn intraplanar and interplanar exchange path lengths in $Ba_xSr_{1-x}LaMnO_4$. The bond-paths are the sums of the bond distances indicated in Fig. 1 b) and c)

x	Intraplanar path length/Å	Interplanar path length/Å
0.06(2)	3.7982(2)	9.256(5)
0.11(2)	3.8033(2)	9.260(5)
0.15(2)	3.8095(2)	9.266(5)
0.21(2)	3.8114(2)	9.278(5)
0.23(2)	3.8169(2)	9.286(5)
0.29(2)	3.8229(2)	9.295(5)
0.34(2)	3.8337(4)	9.302(5)

$SrLaMnO_4$, shows no sign of magnetic long range order. In the solid solution $Ba_xSr_{1-x}LaMnO_4$, one observes a systematic decrease in the ordered moment and T_c up to $x = 0.29$. Mn moments of roughly half the expected value of 4.0 μ_B and T_c near 60 K are found for $x = 0.21$–0.29. A remarkably short 2D correlation length, $\xi_{2D} = 21(3)$ Å is observed just above T_c for the $x = 0.06$ phase. An attempt is made to rationalize these facts, invoking the diminution of ξ_{2D} and J^{inter} with the substitution of the larger Ba^{2+} ion for Sr^{2+} and the presence of competing AF/F exchange interactions.

Acknowledgements

This work has benefited from the use of the Intense Pulsed Neutron Source at Argonne National Laboratory that is funded by the U.S. Department of Energy, BES-Materials Science, under Contract No. W-31-109-END-38. We would like to thank Simine Short for collecting the powder neutron diffraction data at IPNS. We also acknowledge the support of Ian Swainson and the beam time on the powder neutron diffractometer C2 in Chalk River, which is operated by NPMR and NRC, Canada. Financial Support from the Natural Science and Engineering Research Council of Canada (NSERC, J. E. G.) is gratefully acknowledged.

References

1 A. Benabad, A. Daoudi, R. Salmon and G. Le Flem, *J. Solid State Chem.*, 1977, **22**, 121.
2 L. J. de Jongh, *Magnetic Properties of Layered Transition Metal Compounds*, Kluwer Academic Publishers, Boston, MA, 1990.
3 S. Kawano, N. Achiwa, N. Kamegashira and M. Aoki, *J. Phys. (Paris)*, 1988, **49**, C8-829.
4 Y. Morimoto, Y. Tomioka, A. Asamitsu and Y. Tokura, *Phys. Rev. B: Condens. Matter*, 1995, **51**, 3297.
5 Y. Morimoto, T. Arima and Y. Tokura, *J. Phys. Soc. Jpn.*, 1995, **64**, 4117.
6 J. van Elp, H. Sato, T. Kimura, T. Toda, Y. Okamura, Y. Tokura and M. Taniguchi, *J. Phys. Soc. Jpn.*, 2000, **69**, 2391.
7 A. C. Larson and R. B. von Dreele, General Structure Analysis System, Los Alamos National Laboratory, NM, 2000.
8 I. D. Brown and D. Altermatt, *Acta Crystallogr., Sect. B*, 1985, **41**, 244.
9 J. D. Jorgensen, B. Dabrowski, S. Pei, D. G. Hinks, L. Soderholm, B. Morosin, J. E. Schirber, E. L. Venturini and D. S. Ginley, *Phys. Rev. B: Condens. Matter*, 1988, **38**, 11 337.
10 D. E. Rice and D. J. Buttrey, *J. Solid State Chem.*, 1993, **105**, 197.
11 J. B. Goodenough, *Magnetism and the Chemical Bond*, Interscience Publishers, New York, 1963, p. 174.
12 M. F. Collins, *Magnetic Critical Scattering*, Oxford Series on Neutron Scattering in Condensed Matter, Oxford University Press, Oxford, 1989.
13 R. J. Birgeneau, H. J. Guggenheim and G. Shirane, *Phys. Rev. B: Solid State*, 1970, **1**, 2211.
14 B. E. Warren, *Phys. Rev.*, 1941, **59**, 693.
15 J. E. Greedan, M. Bieringer, J. F. Britten, D. M. Giaquinta and H.-C. zur Loye, *J. Solid State Chem.*, 1995, **116**, 118.
16 L. J. de Jongh, *Magnetic Properties of Layered Transition Metal Compounds*, Kluwer Academic Publishers, Boston, MA, 1990, p. 19.
17 M. Vallino, F. Abbattista, D. Mazza and A. Delunas, *Mater. Res. Bull.*, 1986, **21**, 733.
18 A. Delunas, V. Maxia, F. Abbattista, D. Mazza and M. Vallino, *Nuovo Cimento Soc. Ital. Fis., D*, 1986, **8**, 251.